

GEORG-AUGUST-UNIVERSITÄT  
GÖTTINGEN

---

# Project 6: Model for the Spread of Infectious Diseases

---

Carlo von Carnap

Summer Semester 2023

Final Project *Scientific Computing*,  
Salvatore R. Manmana

Supervisor: Emily Klass

Submission Date: 08.08.2023

# Contents

<b>1</b>	<b>Introduction</b>	<b>1</b>
<b>2</b>	<b>Methodology</b>	<b>1</b>
2.1	Pseudorandom Number Generator (PRNG) MT19937 . . . . .	1
<b>3</b>	<b>Implementation</b>	<b>2</b>
3.1	Integration of External Libraries . . . . .	2
3.2	Structure and Workflow of the Main Program . . . . .	2
3.2.1	Generation of Random Numbers by a Static PRNG . . . . .	2
3.2.2	Implementation of the Modelling Grid . . . . .	2
3.2.3	Functions Acting on the Modelling Grid . . . . .	3
3.2.4	Structure of the Main Function and General Workflow . . . . .	3
3.3	Generated Data Files . . . . .	4
<b>4</b>	<b>Results and Discussion</b>	<b>4</b>
4.1	Ratio of Infected People Averaged over Time . . . . .	4
4.2	Influence of Vaccinated People on the Spread . . . . .	5
4.3	Time Evolution of the Infection Rate . . . . .	5
<b>5</b>	<b>Supplementary Materials</b>	<b>9</b>
	<b>Bibliography</b>	<b>10</b>

# 1 Introduction

Infectious disease modelling describes the process of applying mathematical models to predict the future state of an epidemic. Recently it has surged in popularity during the COVID-19 pandemic and its influence on recent policies has been overwhelming, despite its mediocre success in projecting reality. The difficulties when modelling infectious diseases range from the overcomplex real situations to finding suitable assumptions to keep an appropriate level of accuracy. Generally it can be distinguished between macroscale models such as the SEIR-model[1] that apply differential equations on a population level, and microscale models that have individuals as their smallest unit.

This model uses a cellular automaton[2] of quadratic shape  $L \times L$  as well as stochastic methods to examine the spread of an infectious agent on a microscale. Each grid node is occupied by an immobile person and can be in one of the states Susceptible  $S$ , Infected  $I$  or Recovered  $R$ . Later, the forth state Vaccinated  $V$  is introduced, that permanently excludes the respective people from taking any of the three other states. For a person in one of the three active states  $S$ ,  $I$  and  $R$ , the following three transitions are possible,

$$\text{Susceptible } S \xrightarrow{p_1} \text{Infected } I \xrightarrow{p_2} \text{Recovered } R \xrightarrow{p_3} \text{Susceptible } S.$$

With that, we have the following three transition probabilities:

- $p_1$ : a susceptible person getting infected by an infected neighbor,
- $p_2$ : an infected person turning recovered
- $p_3$ : a recovered person returning susceptible

For the  $S \rightarrow I$  transition, a von Neumann neighborhood was applied, meaning the four immediately adjacent nodes are considered as neighbors.[2] Vaccinated people  $V$  are set at the beginning of the simulation, with  $p_4$  being the probability that a spot is occupied by one. The other three states are initialized with the same likelihood, as the simulation steps progress by each updating  $L^2$  randomly chosen nodes according to the above mentioned rules.

Goal was now to use this model to examine the influence of the transition probabilities on the infection rates averaged over all simulation steps. This included varying the  $S \rightarrow I$  turnover rate  $p_1$  for different combinations of  $p_2$  ( $I \rightarrow R$ ) and  $p_3$  ( $R \rightarrow S$ ) as well as using different vaccination rates  $p_4$  at initialization. For all simulations, different grid sizes were used to observe potential statistical inaccuracies.

Further, the time evolution of the infection rates was looked at to stress the validity of the preceding time averaging. Therefore a quantity of 20 infection rate samples was generated over simulation time with mean and standard deviation calculated for each timestep.

## 2 Methodology

### 2.1 Pseudorandom Number Generator (PRNG) MT19937

For the generation of pseudorandom numbers the 1997 developed PRNG Mersenne Twister MT19937[3] was chosen. It was published in 1997 and has become one of the most popular RNGS across programming languages.[4]

Its very long period with  $2^{19937} - 1$  integers as well as the fact that its random numbers are highly equidistributed[5], make the Mersenne Twister a very strong choice. The Mersenne Twister broadly works by first taking a vector of 624 random numbers as seed, that are then transformed applying a “twist” operation and subsequently used to retrieve the usable pseudorandom number. Once all integers of the state vector are consumed, the vector is regenerated.[4][6]

## 3 Implementation

### 3.1 Integration of External Libraries

Alongside the C standard library headers, the `gsl_rng.h` of the GNU Scientific Library (GSL) as well as the two numeric libraries `cvc_numerics.h` and `cvc_rng.h` were included in the project. Of the standard library, the header files `stdio.h`, `stdlib.h`, `tgmath.h` and `time.h` were used, the GSL header `gsl_rng.h` was only accessed to generate pseudorandom numbers.

The `cvc_numerics.h` of the two own libraries provides mainly numerical methods for differentiation, integration or to solve differential equations, while the `cvc_rng.h` offers functions requiring PRNGs like for instance Monte-Carlo integrators or tools helpful to analyse stochastic datasets such as calculating mean or standard deviation of given arrays.

### 3.2 Structure and Workflow of the Main Program

#### 3.2.1 Generation of Random Numbers by a Static PRNG

For the generation of pseudorandom numbers the in Subsection 2.1 described Mersenne Twister MT19937 was used. It was implemented statically to generate uniformly distributed numbers in the interval  $[0, 1)$  and can therefore be accessed globally by the respective functions.

Overall the PRNG was used in two different ways, once to obtain probabilities, other to generate random integers. The former was accomplished by checking if the uniform was smaller than the respective probability, the latter by multiplying the uniform by the largest desired integer and then casting it to `int`.

#### 3.2.2 Implementation of the Modelling Grid

The above mentioned grid itself was realized as a  $(L + 2) \times (L + 2)$  heap section of integer values, with  $L$  being the sidelength of the quadratic grid where the actual spread of the infection takes place. While this section is technically one-dimensional, it will for simplicity reasons be here referred to as a two-dimensional structure of the given shape. Inside the grid, the following integer values were used to model the different states of the people within the simulation:

- 0: this person is Susceptible  $S$  to the infection
- 1: the person is Infected  $I$
- 2: the person is Recovered  $R$  and currently not susceptible
- -1: the person is Vaccinated  $V$  and does not participate in the spread

The grid was implemented with a supporting edge of ghosts at the top, bottom, left and right border, that are neither infectious nor subject to any updates of the grid — they will permanently take the value 0 and are irrelevant for the later visualization and analysis of the data.

### 3.2.3 Functions Acting on the Modelling Grid

In the main program all changes in the grid are facilitated by functions outside the main one. They entirely work with or change the grid in-place and all take the grid itself as well as its length  $L + 2$  as arguments. Inside the functions, the grid is referred to as `grid` and its length as `length`, while the above probabilities are passed in form of the double array `probabilities` having  $p_1, p_2, p_3$ , and  $p_4$  as its entries. Excluding the ones to calculate the infection rate and its time average, none of the functions does have a return value. Overall the following functions can be called from the main:

- `void print_grid`: prints the passed grid as terminal output
- `void grid_init`: initializes the grid applying the vaccination probability
- `void update_node`: updates the given node selected by its  $L \times L$  grid coordinates `row_i` and `column_j` according to the turnover probabilities
- `void grid_update_linear`: calls the `update_node` function for each node in order of their grid position
- `void grid_update_stochastic`: calls `update_node` for  $L^2$  randomly chosen nodes
- `double ratio_infected`: calculates the ratio of infected individuals with respect to the total grid population for a given grid
- `double average_ratio_infected`: applies  $T$  simulation steps to the grid by calling the stochastic grid updater with passed turnover probabilities and averages the calculated infection rate over each simulation step

### 3.2.4 Structure of the Main Function and General Workflow

The main function is divided into sections for each individual analysis step, where every section is an enclosed space in order to prevent the variables from interfering with each other. Therefore each one uses its own variables, files and grids, with the latter being then shaped by calling the functions from Subsection 3.2.3. The files are also being written at directly from the main function.

The first section itself uses the command line interface to take the probabilities  $p_1, p_2, p_3$ , and  $p_4$  as well as the grid size  $L$  as user input. Further it can be specified how the grid is going to be updated. Either all grid nodes are updated sequentially (for user input 0) or  $L^2$  grid nodes are selected randomly. After initializing the grid, individual actualization steps can be performed manually according to the previously selected simulation scheme by pressing `ENTER` until the loop is quit with `q` confirmed by `ENTER`. While here the mechanism to update the grid is subject to the users input, for the following simulation tasks the model operates using the stochastic updating method for each timestep (i.e.  $L^2$  random nodes are selected for actualization). It was chosen to avoid adding a spatial bias by having pre-selected order; however, in terms of results, there is no meaningful difference expected between the two schemes.

The remainder of the program runs independently from the user, **overall a running time of around three minutes should be expected after the interactive part is finished.**

### 3.3 Generated Data Files

Overall, the following files are generated by the main program into the data folder `/soi_data`:

- `soi_average_ratio_infected_over_p1_a.csv`
- `soi_average_ratio_infected_over_p1_b.csv`
- `soi_average_ratio_infected_over_p1_c.csv`
- `soi_average_ratio_infected_over_p4.csv`
- `soi_ratio_over_time.csv`

Additionally, the files of the time evolution of the grid states themselves are created in the `soi_animations` folder:

- `soi_grid_over_time_a.csv`
- `soi_grid_over_time_b.csv`
- `soi_grid_over_time_c.csv`

## 4 Results and Discussion

### 4.1 Ratio of Infected People Averaged over Time

Aim was now to analyse the infection rate inside the grid averaged over all timesteps  $\overline{\langle I \rangle}$  for different combinations of  $p_1$ ,  $p_2$  and  $p_3$ . To achieve this, the dependency of the turnover probability  $p_1$  ( $S \rightarrow I$ ) on the time-averaged infection rates was simulated for different combinations of  $p_2$  ( $I \rightarrow R$ ) and  $p_3$  ( $R \rightarrow S$ ). The simulation was performed over  $T = 1000$  simulation steps for each of the grid sizes  $L = 16$ ,  $L = 32$ ,  $L = 64$  and  $L = 128$ . The latter grid size  $L = 128$  is the largest one used for any simulation and still takes an acceptable but still non-negligible amount of calculation time. Since this side length should provide more than fluctuation-resistant results and the calculation time more than doubles for a doubling in  $L$ , this was the maximum grid size trialed.

From looking at the results shown in Figure 1 it immediately becomes visible that the lower grid sizes undergo stronger fluctuations in  $\overline{\langle I \rangle}$  than the higher ones, with very strong deviations for  $L = 16$ , particularly with  $p_2 = 0.6$  and  $p_3 = 0.3$ . It is worth noting that the lower grid sizes only deviate towards smaller time-averaged infection rates and never towards higher ones. This can be explained by the underlying reason behind the deviations, which is not in fact primarily attributed to statistical fluctuations — those are kept to a minimum due to averaging over time — but rather a secondary effect of the stochastic methods: the spread came to a halt after the number of infected individuals had fluctuated to zero at some point during the simulation. The occurrence of these zeroed runs does obviously happen more frequently with smaller grids, which can be confirmed using the manual updater at the beginning of the program and operating it with even

lower grid sizes such as  $L = 8$ . Since the final time-averaged infection rate also correlates with the timestep where the spread eventually stopped (and earlier halts are more likely with lower infection rates), stronger outliers also follow as more frequent for low infection rates. Consequently the simulation ran with  $p_2 = 0.6$  and  $p_3 = 0.3$  and therefore the lowest  $\langle I \rangle$ , also underwent the biggest changes from  $L = 16$  in comparison with higher grid sizes.

To further focus on the variations for different values of  $p_2$  and  $p_3$  as well as the exact shape of the plotted curves, the time-averaged infection rates  $\langle I \rangle$  for the different probability combinations are shown together in Figure 2. The plots only comprise the grid size  $L = 128$  for better visibility, while the biggest grid size was chosen for accuracy reasons. Qualitatively it can be seen that  $\langle I \rangle$  remains approximately zero until a critical probability  $p_1$  ( $S \rightarrow I$ ) is reached and then experiences a rise leading to a maximum value at  $p_1 = 1$ . The critical value of the the time-averaged infection rate becoming non-zero, as well as the maximum value of  $\langle I \rangle$  differ between the different combinations of  $p_2$  ( $I \rightarrow R$ ) and  $p_3$  ( $R \rightarrow S$ ). Specifically, that means we receive larger maximum values of  $\langle I \rangle$  for likelier  $I \rightarrow R$  transitions and smaller maximum  $\langle I \rangle$  values for likelier  $S \rightarrow I$  turnover rates. This corresponds to the intuitive understanding of the problem: there are more infected individuals when infections occur more frequently (hence the rise in  $\langle I \rangle$  for increased  $p_1$ ) or when people are sooner capable of getting (re)infected and overall less infected individuals for recoveries becoming more likely. For the critical probability  $p_1$  it can be observed that it is significantly higher for a likelier  $I \rightarrow R$  transition but remains approximately the same for the two values of  $p_3$  ( $R \rightarrow S$ ).

## 4.2 Influence of Vaccinated People on the Spread

In this simulation part, permanently vaccinated individuals  $V$  were introduced. To investigate their influence of the infectious spread, the vaccination rate  $p_4$  was varied between zero and one and its influence on the infection rate — again averaged over simulation time — calculated for  $p_1 = p_2 = p_3 = 0.5$ . Like previously, a total of  $T = 1000$  simulation steps for the grid sizes  $L = 16$ ,  $L = 32$ ,  $L = 64$  and  $L = 128$  were conducted and can be seen in Figure 3.

## 4.3 Time Evolution of the Infection Rate

In the preceding subsections the average of the ratio of infected individuals has been taken over time. For this calculation to yield meaningful results, it is necessary to have rather time-stable infection rates over the course of the simulation. For that matter, the focus should now be layed on the time development of the infection rate  $\langle I \rangle_t$  itself. Overall  $N = 20$  samples were generated, while a grid size  $L = 64$  was chosen for appropriate balance between running time and accuracy. The number of simulation steps again was set to  $T = 1000$ . Further, the mean of the infection rates  $\langle I \rangle_t$  and as its standard deviation  $\sigma_{\langle I \rangle_t}$  were calculated for each simulation step. This allows for a more detailed analysis of the statistical fluctuations in the infection rates  $\langle I \rangle_t$  within and across samples.

The results are displayed in Figure 4 and first and foremost show

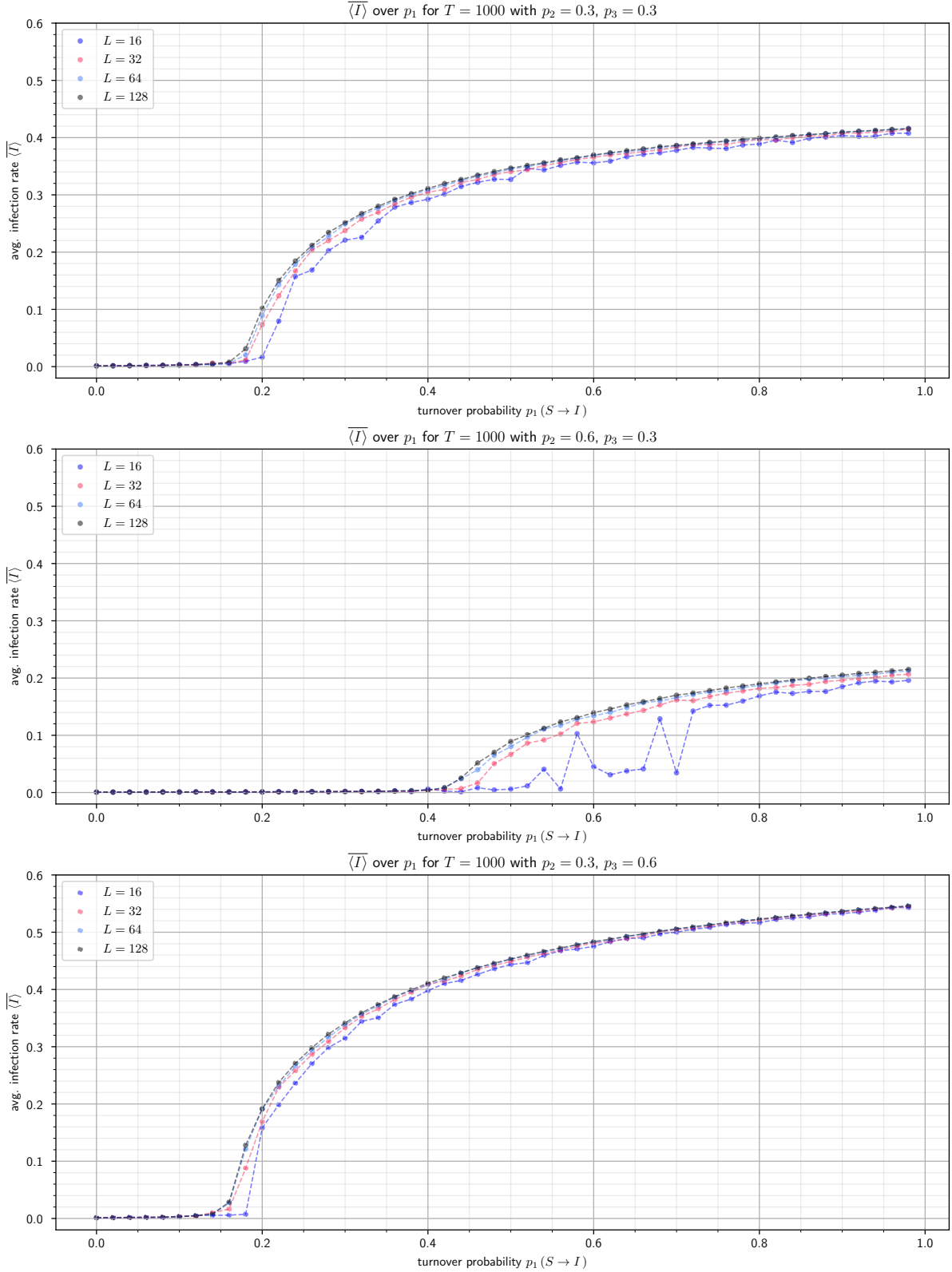


**Figure 1:** Plots showing the time-averaged infection rates  $\overline{\langle I \rangle}$  in dependence of the turnover probability  $p_1$  ( $S \rightarrow I$ ) for the different grid sizes  $L = 16$ ,  $L = 32$ ,  $L = 64$  and  $L = 128$  with  $T = 1000$  simulation steps each. The upper plot shows has now been generated using the turnover rates  $p_2$  ( $I \rightarrow R$ ) = 0.3 and  $p_3$  ( $R \rightarrow S$ ) = 0.3, the middle one using  $p_2 = 0.6$  and  $p_3 = 0.3$ , and the lower one  $p_2 = 0.3$  and  $p_3 = 0.6$ .



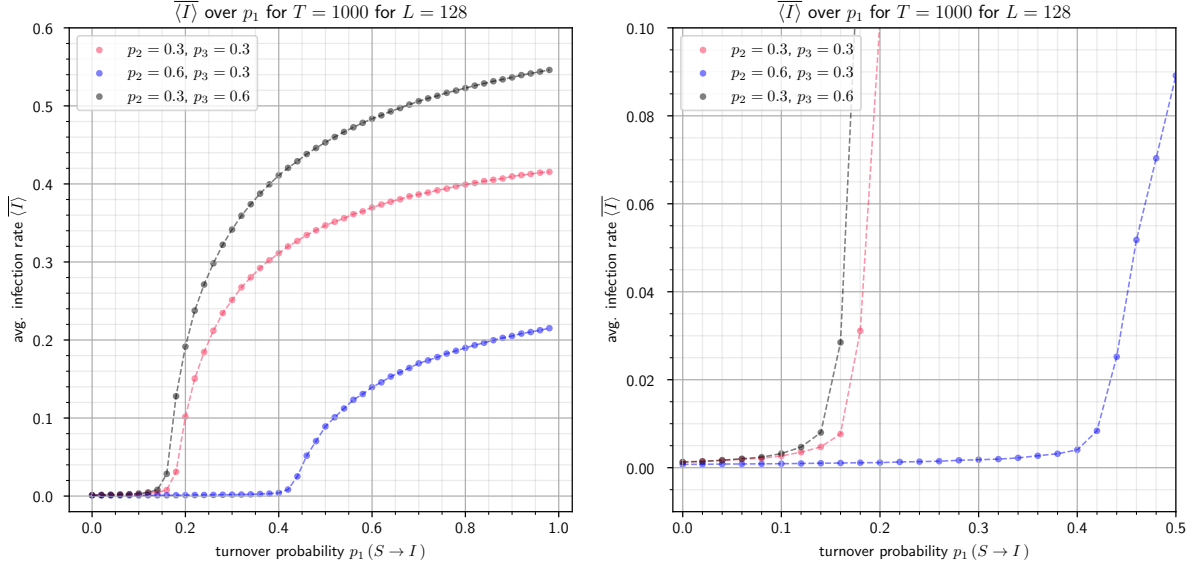


**Figure 2:** Detailed view of the time-averaged infection rates  $\overline{\langle I \rangle}$  over  $p_1 (S \rightarrow I)$  for  $L = 128$  and  $T = 1000$  simulation steps. On the left the different trends for the respective choices of  $p_2 (I \rightarrow R)$  and  $p_3 (R \rightarrow S)$  can be observed, while on the right the critical values of  $p_1$  for  $\overline{\langle I \rangle}$  approaching zero are visible.

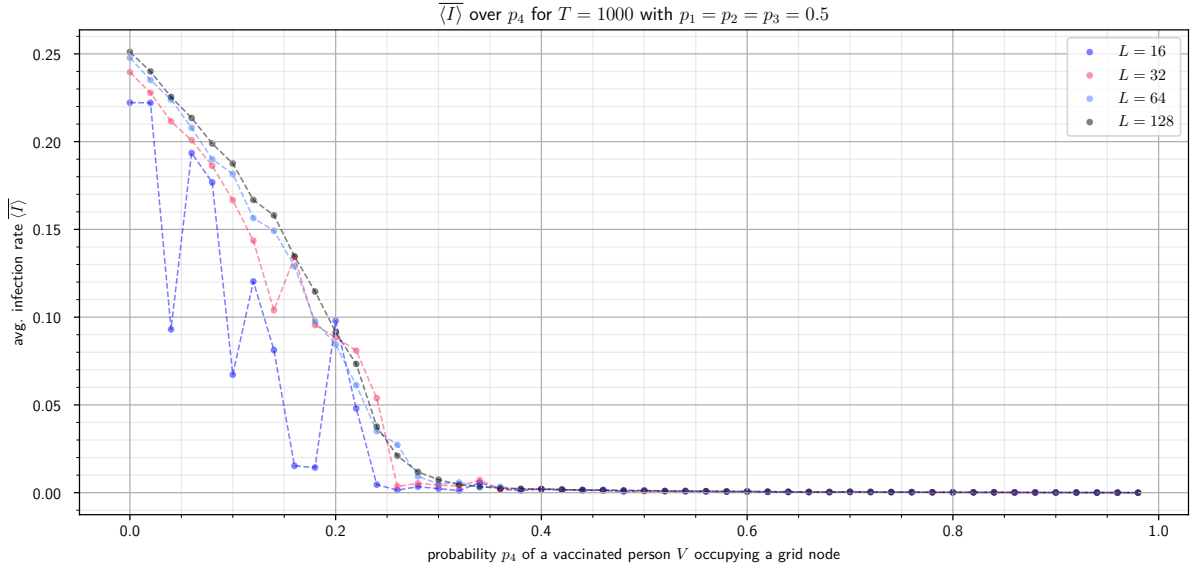


**Figure 3:** Display of the time-averaged infection rates  $\overline{\langle I \rangle}$  depending on the vaccination rate  $p_4$  at the beginning of the simulation and constant turnover probabilities  $p_1 = p_2 = p_3 = 0.5$ . The simulation was performed over  $T = 1000$  simulation steps and the respective grid sizes  $L = 16$ ,  $L = 32$ ,  $L = 64$  and  $L = 128$ .

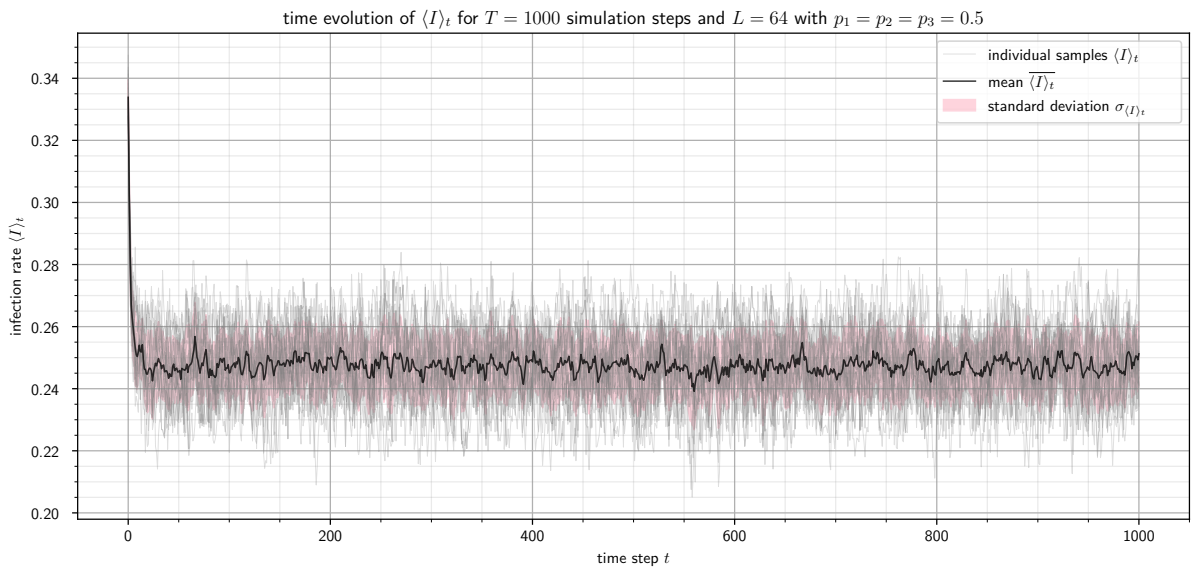


**Figure 4:** Time evolution of the infection rate  $\langle I \rangle_t$  over each of the  $T = 1000$  simulation steps for a total of 20 samples. At each timestep mean  $\langle I \rangle_t$  and standard deviation  $\sigma_{\langle I \rangle_t}$  of the infection rate were calculated and are also displayed in the plot. The grid size was chosen as  $L = 64$ , the turnover probabilities as  $p_1 = p_2 = p_3 = 0.5$ , no vaccinated individuals were used.

## 5 Supplementary Materials

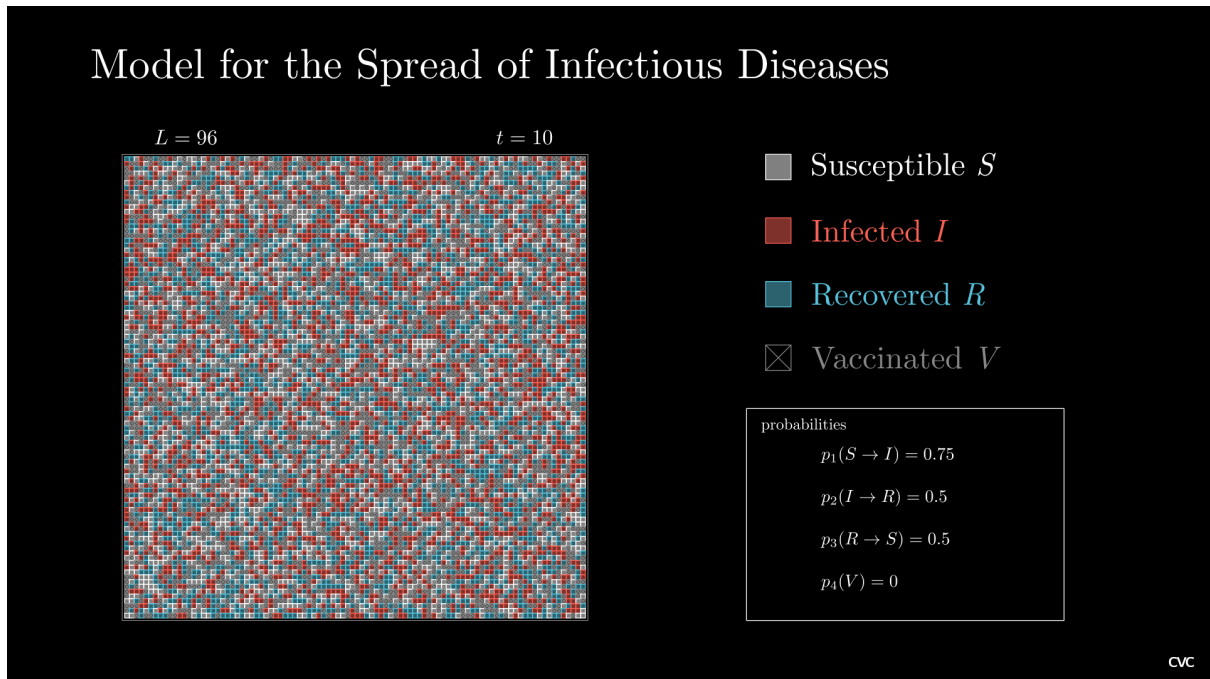


**Figure 5:** Frame  $t = 10$  of an animated simulation of the infectious disease model for the grid size  $L = 96$ . The grid was initialized with a vaccination rate  $p_4 = 0.25$  and progressed with the turnover probabilities  $p_1 = 0.75$  as well as  $p_2 = p_3 = 0.5$ . The total animation as well as variations in the probabilities can be found under `/soi_animations`.

## Literature

- [1] Cornelis P. Dullemond. *EpiDemo. SEIR-Type models*. URL: <https://www.ita.uni-heidelberg.de/~dullemond/software/epidemo/seirmodels.html> (visited on 07/31/2023).
- [2] Debasis Das. “A Survey on Cellular Automata and Its Applications”. In: vol. 269. Dec. 2011. ISBN: 978-3-642-29218-7. DOI: 10.1007/978-3-642-29219-4\_84.
- [3] Makoto Matsumoto and Takuji Nishimura. “Mersenne Twister: A 623-Dimensionally Equidistributed Uniform Pseudo-Random Number Generator”. In: *ACM Trans. Model. Comput. Simul.* 8.1 (1998). ISSN: 1049-3301. DOI: 10.1145/272991.272995. URL: <https://doi.org/10.1145/272991.272995>.
- [4] *educative*. *What is Mersenne Twister?* URL: <https://www.educative.io/answers/what-is-mersenne-twister> (visited on 07/29/2023).
- [5] Alex. *Learn C++. Generating random numbers using Mersenne Twister*. July 28, 2023. URL: <https://www.learncpp.com/cpp-tutorial/generating-random-numbers-using-mersenne-twister/> (visited on 08/02/2023).
- [6] David Wong. *www.cryptologie.net. How does the Mersenne’s Twister work?* Feb. 2016. URL: <https://www.cryptologie.net/article/331/how-does-the-mersennes-twister-work/> (visited on 08/02/2023).